Efficacy of Texture, Shape, and Intensity Feature Fusion for Posterior-Fossa Tumor Segmentation in MRI

Shaheen Ahmed, Khan M. Iftekharuddin, *Senior Member, IEEE*, and Arastoo Vossough

***Abstract*—Our previous works suggest that fractal texture feature is useful to detect pediatric brain tumor in multimodal MRI. In this study, we systematically investigate efficacy of using several different image features such as intensity, fractal texture, and level-set shape in segmentation of posterior-fossa (PF) tumor for pediatric patients. We explore effectiveness of using four different feature selection and three different segmentation techniques, respectively, to discriminate tumor regions from normal tissue in multimodal brain MRI. We further study the selective fusion of these features for improved PF tumor segmentation. Our result suggests that Kullback–Leibler divergence measure for feature ranking and selection and the expectation maximization algorithm for feature fusion and tumor segmentation offer the best results for the patient data in this study. We show that for T1 and fluid attenuation inversion recovery (FLAIR) MRI modalities, the best PF tumor segmentation is obtained using the texture feature such as multifractional Brownian motion (mBm) while that for T2 MRI is obtained by fusing level-set shape with intensity features. In multimodality fused MRI (T1, T2, and FLAIR), mBm feature offers the best PF tumor segmentation performance. We use different similarity metrics to evaluate quality and robustness of these selected features for PF tumor segmentation in MRI for ten pediatric patients.**

***Index Terms*—Expectation maximization (EM), fractal dimension (FD), Kullback–Leibler divergence (KLD), MRI modalities, multi-fractional Brownian motion (mBm).**

I. Introduction

BRAIN tissue and tumor segmentation in MR images have been an active research area. Extraction of good features is fundamental to successful image segmentation. Due to complex structures of different tissues such as the gray matter (GM), white matter (WM), and cerebrospinal fluid (CSF) in the MR brain images, extraction of useful features is a challenging task. Variability in tumor location, shape, size, and texture properties further complicates the search for robust features. Posterior-fossa (PF) tumor is usually located near the brain stem and cerebellum. About 55–70% pediatric brain tumors arise in the PF. Due to narrow confinement at the base of the skull, complete removal of PF tumors poses nontrivial challenges. Therefore, accurate segmentation of PF tumor is necessary.

Intensity is an important feature in segmenting tumor from other tissues in the brain [1]. However, using intensity alone for segmentation has proved to be insufficient. Fractal dimension (FD) is a useful tool to characterize the textured images and surface roughness [2]. FD has been exploited to quantify cortical complexity of the brain [3]. Further, texture feature obtained using a stochastic multifractional Brownian motion (mBm) model is shown effectively to segment brain tumor [4]. In our previous works [4]–[7], we discuss the usefulness of intensity, FD, and mBm wavelet fractal texture features for tumor segmentation. However, for patients with poor MRI quality, the texture and intensity features may prove inadequate for PF tumor segmentation. For these patients, another feature such as the shape may be useful for improved PF tumor segmentation in MRI.

The level-set method first developed by Osher and Sethian [8] has found applications in many disciplines. The level set is a numerical analysis technique for tracking interfaces and shape. Some applications of level sets in medical image analysis are extraction of complex shapes such as the human cortex in MRI for neurological disease diagnosis and shape-based approach to curve evolution for the segmentation of medical images [9]. In a recent work [10], a binary level-set method has been introduced to reduce the expensive computational cost of redistancing the traditional level-set function.

Feature selection, on the other hand, is a technique for selecting a subset of relevant features for building robust learning models. Feature selection has been exploited in many applications such as medical imaging, data mining, and lexical works. In medical imaging, various techniques have been used to select the best features from a given set of features [11], [12]. The Kullback–Leibler divergence (KLD) is one such feature selection technique between two-class conditional density functions approximated by finite mixture of parameterized densities [12].

In our current study, we evaluate the efficacy of the level-set shape along with fractal texture and intensity features to discriminate PF tumor from other tissues in the brain. We investigate the efficacy of these features using different feature ranking and selection techniques such as entropy and KLD along with different feature fusion and segmentation methods such as graph

Manuscript received September 9, 2009; revised June 25, 2010 and September 24, 2010; accepted December 23, 2010. Date of publication January 6, 2011; date of current version March 4, 2011. This work was supported in part by the Whitaker Foundation through biomedical engineering research under Grants RG-01-0125 and TG-04-026 and in part by the NIH/NCI research under Grant 1R15CA115464.

S. Ahmed is with the Department of Electrical and Computer Engineering, University of Memphis, Memphis, TN 38152 USA (e-mail: sahmed1@memphis.edu).

K. M. Iftekharuddin is with the Department of Electrical and Computer Engineering, University of Memphis, Memphis, TN 38152 USA, and also with the University of Tennessee, Memphis, TN 38163 USA (e-mail: iftekhar@memphis.edu).

A. Vossough is with Pediatric Radiology, Children Hospital of Philadelphia, PA 19104 USA (e-mail: vossough@email.chop.edu).

Color versions of one or more of the figures in this paper are available online at http://ieeexplore.ieee.org.

Digital Object Identifier 10.1109/TITB.2011.2104376

cut and expectation maximization (EM) for PF brain tumor segmentation using the selected features.

II. Background Review

In this section, we first review relevant background for feature extraction using fractal, multifractal texture, and level-set shape methods. The tumor growth is known to follow a fractal process [13] that can be quantified using FD. The FD can be used as a measure of degree of the texture complexity of the tumor surface. Among many other conventional feature extraction methods, the Gabor filters are suitable to capture discontinuity in intensity and texture in an image [14]. Gabor-wavelet filters have been investigated to outline the area of metaplastic changes in cervical images [15], and also to differentiate prostate and nonprostate tissues [16]. However, the Gabor-wavelet technique does not provide an integrated mathematical framework for simultaneous analysis of tumor texture at different resolutions. In comparison, wavelet-fractal techniques capture the multiresolution and texture features simultaneously for effective tumor segmentation [5]–[7], [17].

From many different types of features such as intensity, texture, multiresolution texture and shape, some features may be redundant or irrelevant for PF tumor segmentation. Therefore, it is essential to perform systematic feature ranking and selection. Following different feature selection techniques, neural networks (NN) [18] have attracted attention. However, NN-based feature selection is an exhaustive search method; hence, it may be computationally expensive. Another hybrid technique that uses classifiers is known as boosting [19]. In addition, simple techniques such as principal component analysis (PCA) [20] have also been used for feature selection. On the other hand, the KLD provides a quantitative feature ranking considering the entropy gain of features. In this study, we systematically investigate four different feature selection techniques such as KLD, PCA, boosting, and entropy to ascertain which features offer the maximum separability between PF tumor and nontumor tissues. Similarly, for feature fusion and segmentation, there have been various methods reported in the literature such as top down and bottom up [21] and graph cut [22]. In addition, the EM algorithm is an efficient iterative feature fusion and segmentation procedure to compute the maximum likelihood estimate in the presence of missing or hidden data [23]. Note that KLD and EM can be combined in a single mathematical framework for feature selection and segmentation. In this study, we explore effectiveness of three different feature fusion and segmentation techniques such as EM and graph cut, respectively.

A. FD Texture Feature Extraction

The concept of fractal is first proposed by Mandelbrot [24] to describe the geometry of the objects in nature. The FD is a real number that characterizes the fractalness (texture) of the objects. We investigate effectiveness of three different FD computation methods for brain tumor segmentation in MRI [7], [25]. In a prior work [25], we demonstrate that the piecewise-triangular-prism-surface area (PTPSA) method offers the most reliable FD values and resulting tumor segmentation.

B. mBm Texture Feature Extraction

We have successfully investigated mBm-based texture model for brain tumor segmentation in MRI [6]. The mBm is defined as [26]

$$x(at) = a^{H(t)}x(t) \tag{1}$$

where $x(t)$ is an mBm process, $H(t)$ is the time-varying scaling (or Holder) exponent, and a is the scaling factor. A series of mathematical derivation leads us to obtain the expectation of the squared magnitude of the wavelet transform W_x of x (t) given as

$$\log(E[|W_x(t,a)|^2]) = (2H(t)+1)\log a + \text{constant}. \tag{2}$$

The critical research issue is to obtain a robust estimation of the expectation of the squared magnitude of the wavelet coefficients given a single observation of the random process x. Following Goncalves [27], the empirical estimate of the qth-order moment of $|W_x(t,a)|$ can be estimated as

$$E\{|W_x(t,a)|^q\} = \frac{1}{N}\sum_{i=0}^{N-1}|W_x(t_i,a)|^q \tag{3}$$

where single realization of the analyzed process is sampled on a uniform lattice $t_i = i/N (i = 0, \ldots, N-1)$. For a 2-D mBm model, let $z(\vec{u})$ represent a 2-D mBm process, where $\vec{u}$ denotes the vector position (u_x, u_y) of a point in the process. Following the similar derivations for (2), we approximate $H(\vec{u})$ for a 2-D mBm process as follows [6]:

$$2H(\vec{u}) = \lim_{a\to 0}\frac{\log\left((1)\backslash(M+N)\sum_{x=0}^{N-1}\sum_{y=0}^{M-1}|W_z(b_{x,y},a)|^2\right)}{\log a}. \tag{4}$$

Finally, FD is obtained as

$$\text{FD} = E + 1 - H \tag{5}$$

where E is Euclidean dimension of the space of fractal ($E = 2$ for a 2-D image) and $H(\vec{u})$ is the Hurst coefficient.

C. Level-Set-Based Shape Feature Extraction

Level-–set-based shape modeling is an important research topic in computer vision and computer graphics. In this study, we implement a more recent work [10] on binary level-set representation for object shape detection. Consider the basic definition of level set given as [4]

$$\phi_t + F|\nabla\phi| = 0, \quad \text{given} \;\; \phi(x, t=0) \tag{6}$$

and

$$\phi_t + F_o\,|\nabla\phi| + U(x,y,t)\nabla\phi = \varepsilon K\,|\nabla\phi| \tag{7}$$

where $F_o\,|\nabla\phi|$ is the motion of the curve in the direction normal to front, $U(x,y,t)\nabla\phi$ is the term that moves the curve across the surface, and $\varepsilon K\,|\nabla\phi|$ is the speed term dependent upon curvature. In our study, $U(x,y,t)$ is the gradient of image and $\varepsilon K\,|\nabla\phi|$ is approximated using a central difference. We first

convert the MRI to binary image. The level set is used on these binary images to track the shape at the boundary of images. Note for binary images, only digital derivative approximations exist at the boundary. We initialize the level-set function using the gradient of the image. We propagate this gradient across the surface given as [10]

$$\phi_{ij}^{t+1} = \phi_{ij}^{t} - \Delta t[\max(G_{ij},0)\Delta^{+} + \min(G_{ij},0)\Delta^{-}] \quad (8)$$

where ϕ_{ij}^{t} is the value of ϕ at pixel *i* at time *t*, Δt is the time step (or scaling factor), G_{ij} is a Gaussian filter to smooth the edges, and Δ^{+} and Δ^{-} describe the normal component and are given as

$$\Delta^{+} = [\max(D_x^{-},0)^2 + \min(D_x^{+},0)^2 + \max(D_y^{-},0)^2 + \min(D_y^{+},0)^2]^{1/2} \quad (9)$$

and

$$\Delta^{-} = [\max(D_x^{+},0)^2 + \min(D_x^{-},0)^2 + \max(D_y^{+},0)^2 + \min(D_y^{-},0)^2]^{1/2} \quad (10)$$

where $D_x^{-}, D_x^{+}, D_y^{-}, D_y^{+}$ are the forward and backward derivative approximation in *x*- and *y*-directions. The Gaussian filter creates a larger attraction range allowing the level sets to be attracted to the boundary. These steps iterate and stop when the boundary is completed upon convergence.

D. KLD for Feature Selection and Entropy for Feature Ranking

The KLD is a measure of difference between two probability distributions [12]. Therefore, KLD can be used for multivariate normal distributions, approximated for the class conditional distributions of the tumor and nontumor regions in MR brain images. The equation for the parametric model for the ωth class conditional density function for a random variable *x* is given as [12]

$$p(x|\omega|) = \sum_{m=1}^{M\omega} \alpha_m^{\omega} g_o(x|\mu_o,\sigma_o) g(x|\mu_m^{\omega},\sigma_m^{\omega},\mu_o,\sigma_o,\theta) \quad (11)$$

where

$$g_o(x|\mu_o,\sigma_o) = \prod_{i=1}^{D}\left[\frac{1}{\sqrt{2\pi}\sigma_{oi}}\exp\left\{\frac{-1}{2}\left(\frac{x_i-\mu_{oi}}{\sigma_{oi}}\right)^2\right\}\right] \quad (12)$$

and

$$g_o(x\,|\mu_m^{\omega}\,,\sigma_m^{\omega},\mu_o,\sigma_o,\theta) = \prod_{i=1}^{D}\left[\frac{\sigma_{oi}}{\sigma_{mi}^{\omega}}\exp\left\{\frac{-1}{2}\left(\frac{x_i-\mu_{mi}^{\omega}}{\sigma_{mi}^{\omega}}\right) + \frac{1}{2}\left(\frac{x_i-\mu_{oi}}{\sigma_{oi}}\right)^2\right\}\right]^{\theta i}. \quad (13)$$

(μ_o,σ_o) is the mean and variance for first class, (μ_m,σ_m) is the mean and variance for the second class, θ is the control parameter, α_m^{ω} is a nonnegative weight, $\sum_{m=1}^{M_\omega}\alpha_m^{\omega} = 1$, and M_ω is the number of features component. We now consider the maximum likelihood estimation of all the unknown parameters such as $A = A_\omega, B = B_\omega, \mu_o$, and σ_o in the parametric family. We use the EM algorithm to maximize the log likelihood function w.r.t. parameters $A, B, \mu_o,$ and σ_o with given θ. The KLD between two classes ω_1 and ω_2 is given as [15]

$$J_i^{\omega} = \frac{1}{2}\left\{\sum_{m=1}^{M_\Omega}\alpha_m^{\omega}\log\left(\frac{1}{\sigma_{mi}^{\omega}}\right)^2 - 1 + \sum_{m=1}^{M_{\Omega-\omega}}\alpha_m^{\omega,\Omega-\omega} \times \left[\log(\sigma_{mi}^{\Omega-\omega})^2 + \left(\frac{\sigma_{mi}^{\Omega-\omega}}{\sigma_{mi}^{\omega,\Omega-\omega}}\right)^2 + \left(\frac{\mu_{mi}^{\omega,\Omega-\omega}-\mu_{mi}^{\Omega-\omega}}{\sigma_{mi}^{\Omega-\omega}}\right)^2\right]\right\} \quad (14)$$

where

$$\mu_{mi}^{\omega} = \sum_{x\in X\omega} x_i g(x|\mu_o,\sigma_o,\omega) \quad (15)$$

$$\mu_{mi}^{\omega,\Omega-\omega} = \sum_{x\in X\omega} x_i g^{\omega}(x|\mu_o,\sigma_o,\Omega-\omega) \quad (16)$$

$$(\sigma_{mi}^{\omega})^2 = \sum_{x\in X\omega}(x_i-\mu_{mi}^{\omega})^2 g(x|\mu_o,\sigma_o,\omega) \quad (17)$$

$$(\sigma_{mi}^{\omega,\Omega-\omega})^2 = \sum_{x\in X\omega}(x_i-\mu_{mi}^{\omega,\Omega-\omega}) g^{\omega}(x|\mu_o,\sigma_o,\Omega-\omega) \quad (18)$$

and

$$J_i = \sum_{i=1}^{D}\theta_i J_i^{\omega}. \quad (19)$$

KL divergence (X, N, k. Ji)
X is the input matrix of size n x1. N is the number of features/dimensions. K is the desired number of clusters.

1. Compute the weights $g_0(x|\mu_0,\sigma_0)$ *and* $g_0(x|\mu_m,\sigma_m)$ *using Eqns. (11) and (12)*

2. Under fixed weights compute the value of μ_{mi}^{ω}, $(\sigma_{mi}^{\omega})^2$, $\mu_{mi}^{\omega,\Omega-\omega}$, $(\sigma_{mi}^{\omega,\Omega-\omega})^2$ *using Eqns.(14)-(17)*

3. Using the parameters of μ_{mi}^{ω}, $(\sigma_{mi}^{\omega})^2$, $\mu_{mi}^{\omega,\Omega-\omega}$, $(\sigma_{mi}^{\omega,\Omega-\omega})^2$ *and weights compute the value of the KLD using Eqn. (18)*

4. Compute the entropy using Eqn.(19)

Fig. 1. Algorithm for computing the feature selection and ranking [12].

Fig. 1 shows the formal algorithm for KLD computation.

We exploit the concepts in information theory such as mutual information and KLD for feature ranking and selection. The mutual information can also be understood as the expectation of the KLD of the univariate distribution $p(x)$ of X from the conditional distribution $p(xc)$ of X given C. This suggests that the more different the distributions $p(xc)$ and $p(x)$, the greater is the information gain, $I(x,c)$, which is given as follows:

$$I(x,c) = E_{xp}\{D_{\mathrm{KL}}(p(x\,|c)\,\|p(x)\} \ . \quad (20)$$

According to feature ranking based on information, gain ranks feature *X* over feature *Y* if Gain (*X, C*) > Gain (*Y, C*). Therefore, a feature should be ranked if it can reduce more entropy than the other. We find the entropy for all the four features—intensity, mBm, fractal, and shape—using (20).

E. Similarity Coefficient for Segmentation Quality and Robustness Identification

For estimating the robustness of segmentation, we consider different similarity measures such as Jaccard, Dice, Sokal and Sneath (SS), and Russel and Rao (RR) [28]. Note that the study of outlier and its effect on segmentation and pattern classification is better understood using region of curves analysis, which is beyond the scope of this study. We quantify segmentation robustness by measuring the overlap of tumor using different similarity metrics such as Jaccard ($p/p+q$), Dice ($2p/2p+q$), SS ($p/p+2r$), and RR ($p/p+q+r$), where p is the area of the tumor region in MRI (tumors segmented by radiologist and used as ground truth), q is the area of the tumor region segmented using the EM algorithm, and r is the nontumor region. Note that computations of both Dice and Jaccard involve the ratio between actual and automated tumor segments. On the other hand, SS and RR involve computations of both the ratio between actual tumor segments to automated tumor segments and the nontumor regions. Overall, these metrics indicate the accuracy of tumor segmentation results for each patient. A value of 1.0 for any of these measures represents complete overlap whereas 0.0 represents no overlap.

III. Methods and Datasets

The overall flow diagram our method is shown in Fig. 2. The first step includes the preprocessing stage that minimizes intensity bias using a normalization algorithm. After preprocessing step, we extract four features such as intensity and FD using PTPSA algorithm, mBm using fractal-wavelet algorithm, and shape using level-set method in multimodality MR images. We use both KLD and the entropy values for feature ranking and selection. The features selected are then used for the segmentation of the tumor region in MRI using EM.

A. Image Intensity Normalization

The MRI intensity is affected by various sources of variations such as different parameter settings and physics of imaging device. To minimize the intensity bias of the MRI, intensity normalization is used as a preprocessing step. In this study, we implement a two-step normalization method in [5] and [6] where the image histograms are modified such that the histograms match a mean histogram obtained using the training data.

B. Feature Extraction

After intensity normalization and bias correction, we extract four sets of features from the normalized images in T1, T2, and FLAIR MRI modalities.

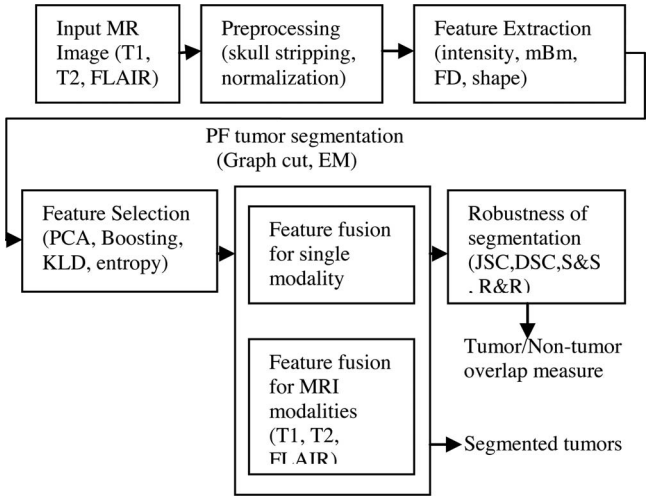

Fig. 2. Flow diagrams showing the steps.

C. Feature Selection and Feature Ranking Using Different Methods

The authors in [20] propose a novel PCA-based method for dimensionality reduction of features known as principal feature analysis (PFA). The PFA has been successfully applied for choosing the principal features in face tracking and content-based image retrieval problems. Similarly, a boost feature subset selection (BFSS) method has been proposed to select and rank genes in microarray data on the basis of discriminative scores to improve the performance [19]. For BFSS implementation, we compute the *F*-score for each feature type in each modality. We then rank the *F*-scores in the descending order. For comparison, we also formalize the mathematical derivation of KLD and use KLD for ranking and selecting the best feature combinations among four features for tumor/nontumor discrimination.

D. Image Segmentation Using Different Algorithms

We study three different segmentation techniques for comparison. For the graph cut method [22], the image is considered a graph and nodes i and j are pixels. Note that the edge weight W_{ij} denotes a local measure of similarity between two pixels. Let $G=\{V, E\}$ where V stands for the node and E for edges. The similarity between two groups is called a cut and is given by

$$\mathrm{cut}(A,B)=\sum_{i\in A, j\in B} W_{ij}. \tag{21}$$

In our study, we compute the edge weights W_{ij} between the two pixels as follows:

$$W_{ij}^{TX}=\exp\left(\frac{||FD_i-FD_j||}{FD_i+FD_j}+\frac{||\mathrm{mBm}_i-\mathrm{mBm}_j||}{\mathrm{mBm}_i+\mathrm{mBm}_j}+\frac{||\mathrm{shape}_i-\mathrm{shape}_j||}{\mathrm{shape}_i+\mathrm{shape}_j}\right) \tag{22}$$

where $W_{ij}=W_{ij}^{TX}$. We compute the eigenvectors by using Laplacian matrix, and use the eigenvector with the second

TABLE I
MRI DATA STATISTICS

Patient	Field Strength (Tesla)	# of tumor	Tumor type	# of images with visible tumors	T1 modality			T2 modality		FLAIR modality	
					Total # of images in a sequence	Tumor visibility	Contrast (GAD applied)	Total # of images in a sequence	Tumor visibility	Total # of images in a sequence	Tumor visibility
1	1.5	Single	Medullo blastoma	9	35	Good	Yes	35	Good	35	Medium
2	1.5	Single	Medullo blastoma	9	35	Medium	Yes	35	Good	35	Medium
3	1.5	Single	Medullo blastoma	9	35	Medium	Yes	35	Medium	34	Good
4	1.5	Single	Medullo blastoma	8	37	Medium	Yes	36	Medium	36	Medium
5	1.5	Single	Medullo blastoma	9	35	Medium	Yes	35	Medium	34	Good
6	1.5	Single	Astrocyt oma	8	40	Good	Yes	40	Good	34	Medium
7	1.5	Single	Astrocyt oma	6	27	Medium	Yes	27	Medium	25	Medium
8	1.5	Single	Astrocyt oma	8	37	Poor	Yes	38	Medium	35	Medium
9	1.5	Single	Astrocyt oma	7	21	Medium	Yes	26	Medium	25	Good
10	1.5	Single	Astrocyt oma	9	28	Medium	Yes	27	Medium	26	Good

smallest eigenvalues computed using Laplacian matrix to bi-partition the graph using (22).

For the EM algorithm, at each pixel in an image, we compute a d-dimensional feature vector that encapsulates intensity and texture information. The EM algorithm assumes that a segment is chosen with a probability, and models the density associated with that segment as a Gaussian probability distribution function, with parameters (μ, σ), that depend on the chosen segment [23]. The EM tool also yields the cluster mean and covariance, for a user-defined number of clusters and number of iterations. Note that varying the number of clusters and the number of iterations influences the computation time and the quality of results. In our study, we randomly initialize the number of clusters and retain the meaningful number of clusters after couple of iterations.

E. Image Dataset

The image database includes the two image modalities—gadolinium-enhanced T1, T2, and FLAIR from ten patients with PF tumors as shown in Table I. All the images are sampled by 1.5 Tesla Siemens Magnetom scanners. The slice thickness is 5 mm, with the slice gap of 1 mm, the field-of-view of 210 mm $\times$ 210 mm, and the image matrix of 256 $\times$ 256 pixels. The scan parameters for T1-weighted image are TR = 168 ms, TE = 8 ms, and flip angle = 90°; the scan parameters for T2-weighted image are Turbo Spin Echo, TR = 6430, TE = 114 ms, and 14 echoes per TR.

IV. RESULTS

A. Feature Extraction and Selection

We compute intensity, FD, fractal wavelet, and shape features in all MRI for ten patients. We first divide the images into 8 $\times$ 8 subimages and obtain the corresponding features using PTPSA, mBm, and level-set algorithms, respectively. Note in our previous work, we show that the effectiveness of fractal algorithms improves by dividing images into 8 $\times$ 8 subimages for the local detection of tumor [4].

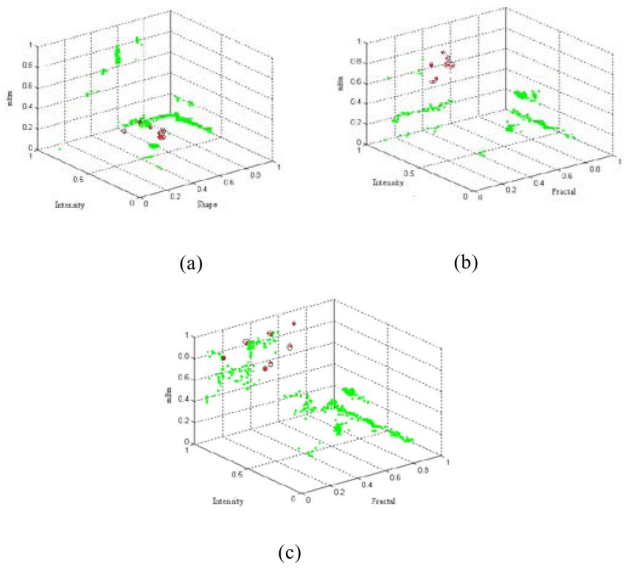

Fig. 3. KLD results showing the separability of features for (a) T1; (b) T2; (c) FLAIR modalities for patient #8. Encircled dots show tumors and the rest shows nontumor.

We then obtain the normalized mean value of the FD, mBm, intensity, and shape features for both tumor and nontumor regions for each MRI slice.

For robust identification of effective features, we investigate feature selection using four different techniques such as PCA, boosting, KLD, and entropy. Fig. 3 shows KLD results in T1, T2,

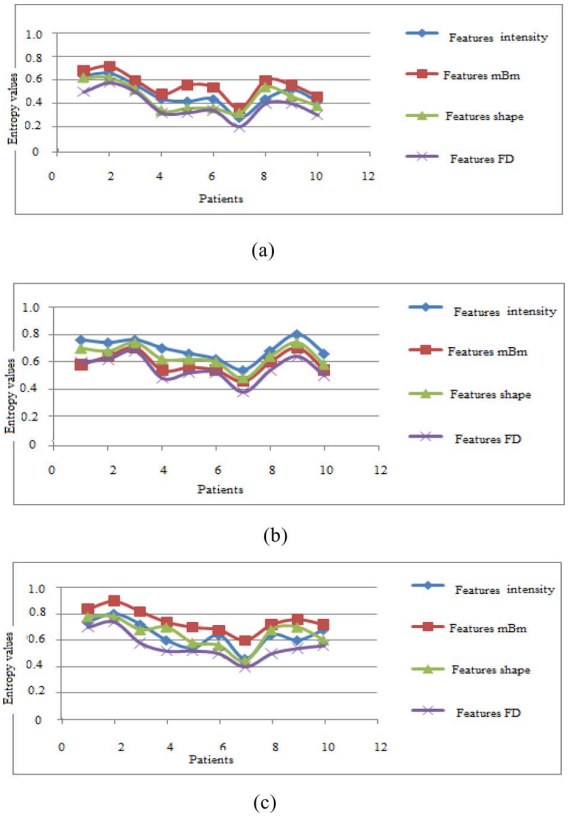

Fig. 4. Summary of entropy-based feature ranking in (a) T1; (b) T2; and (c) FLAIR modalities.

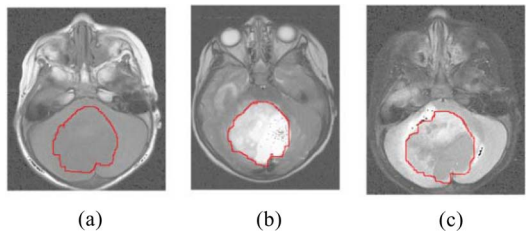

Fig. 5. Example MRI slice for (a) T1; (b) T2; and (c) FLAIR modalities for patient #8. Tumors have been shown using boundary.

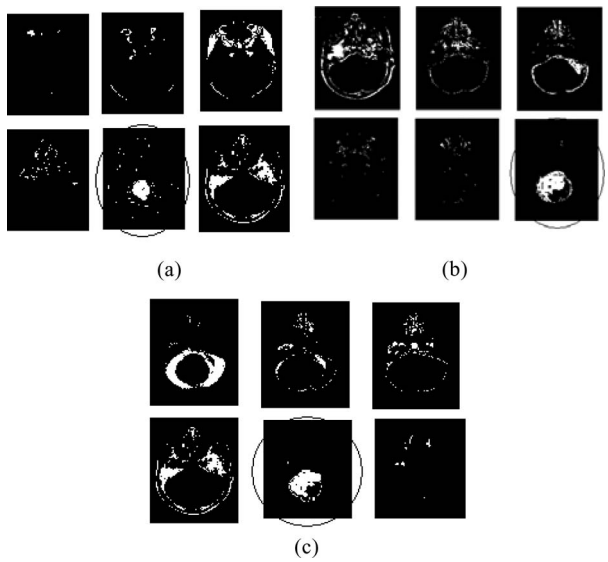

Fig. 6. PF tumor segmentation using EM for patient #8 in (a) T1 image using mBm; (b) T2 image using intensity; and (c) FLAIR image using mBm. Tumor segments are circled.

and FLAIR modalities for patient #8 as an example. Fig. 3(a) and (c) shows that the entire tumor cluster is located in the mBm plane. Thus, mBm can be used to effectively discriminate between the PF tumors and nontumor tissues in T1 and FLAIR MRI. Fig. 3(b) shows that intensity is necessary to isolate tumor cluster in T2. This similar trend is noted for all the ten patients in our database. In order to obtain a more quantitative measure of feature effectiveness, we obtain the entropy (or information gain) for all the four features in T1, T2, and FLAIR modalities, respectively. We then rank these entropies in decreasing order.

Fig. 4 summarizes our ranked entropy results for all ten patients. We observe that in T1 and FLAIR modalities mBm ranks first. In T2 modality, intensity ranks first for all the ten patients. Consequently, using both qualitative KLD features in Fig. 3 and quantitative entropy ranking in Fig. 4, we conclude that mBm is the most effective feature in T1 and FLAIR modalities while intensity is the best for T2 modality. We use the best features obtained using KLD method such as mBm, intensity, and mBm for T1, T2, and FLAIR modalities, respectively, for subsequent processing.

B. PF Tumor Segmentation Using Selected Features

For effective comparison and evaluation, we employ two different tumor segmentation techniques such as graph cut and EM. Fig. 5 shows an example for patient #8 in three MRI modalities. Finally, we obtain tumor segmentation results for the same selected combinations of the features in single modality MRI using EM. Fig. 6(a)–(c) shows the tumor segmentation using mBm in T1, intensity in T2, and mBm in FLAIR, respectively.

In order to compare EM and graph cut methods, we obtain the summary segmentation results (manual% of the area overlap between known ground truth and automated segmentation) for all ten patients in Fig. 7. We further fuse features in T1, T2, and FLAIR MR modalities for tumor segmentation for each patient. Comparison of Fig. 7(a) and (b) confirms that EM is a better segmentation algorithm. Therefore, we employ EM for the next experiment for robustness of tumor segmentation computation.

C. Quality and Robustness of Tumor Segmentation

In order to verify the quality and robustness of our proposed techniques, we obtain four different similarity measures for automatic computation of overlap between tumors segments obtained using EM and ground truth obtained using manual segmentation by radiologists. Fig. 8 shows radar plots for four similarity metrics such as Jaccard, Dice, (SS), and (RR) in T1, T2, and FLAIR modalities for all ten patients, respectively. In each subplot, for a specific metric the values in y-axis represent the overlap coefficient while the axis at each clock location represents the patient number. In Fig. 8(a) and (d), both the overall Jaccard and RR overlap is about 60% for all patients. We

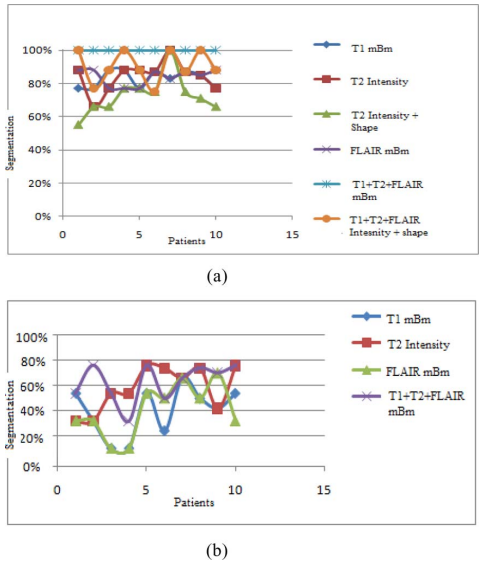

Fig. 7 Summary of tumor segmentation results for (a) EM and (b) graph cut methods.

observe that the Dice overlap in Fig. 8(b) is above 80% for all patients. In Fig. 8(c), SS overlap for nine patients is above 60% except for a dip at 47% for patient #1 for all modalities. Note these results suggest that our techniques perform better when we compare tumor segments obtained using ground truth to that using our automated segmentation technique as indicated by the Dice metric. However, inclusion of nontumor segments in the metrics computations, as indicated by both SS and RR metrics, suggests moderate segmentation performance.

V. Conclusion and Future Work

We systematically investigate the efficacy of different types of features including texture (such as FD and mBm) level-set shape and intensity for segmentation of PF tumors. For selection of the best feature, we compare four different techniques such as PCA, boosting, KLD, and entropy metrics. We implement an integrated mathematical framework for feature selection and ranking using KLD since KLD offers the best feature selection performance for this study. Our KLD feature selection technique shows that mBm is the best feature for both T1 and FLAIR modalities while intensity is for T2 modality. In order to obtain robust segmentation of PF tumor in pediatric brain MRI, we compare performance of three different techniques such as bottom up top down, graph cut, and EM. We finally select an integrated KLD–EM framework for tumor segmentation since this specific combination offers the best performance among the techniques investigated in this study. The uniqueness of our formal KLD computation takes into account the mean and variance of two different classes expressed in terms of EM. We evaluate robustness of our proposed model using four different similarity metrics and demonstrate the efficacy of our technique using 249 real MRI from ten pediatric patients. Furthermore, we show that fusion of mBm feature in multimodalities T1, T2, and FLAIR MRI can offer 100% PF tumor segmentation for the patient cases studied in this study.

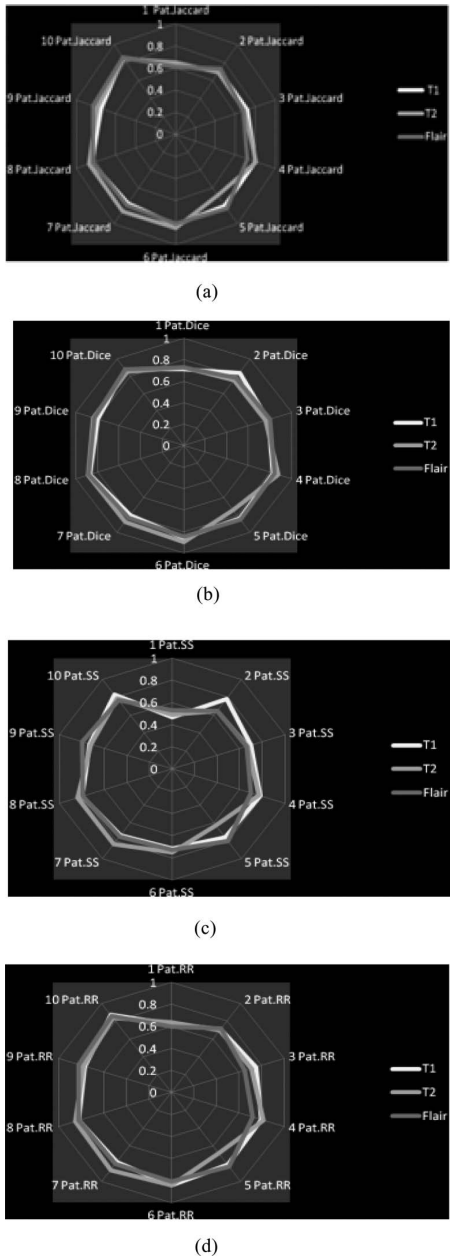

Fig. 8. Plot of similarity metrics for ten patients in three modalities for (a) Jaccard; (b) Dice; (c) Sneath and Sokal (SS); and (d) Russell and Rao (RR). The number outside the circle shows the patient number from 1 to 10. Numbers 0, 0.2, 0.4, 0.6, 0.8, and 1.0 show the range of metrics.

We obtain time estimates of all the steps in this study as shown in Fig. 2 such as normalization, feature extraction, features selection, and segmentation. In our study, the time taken for normalization is 10 min, extraction of all four features is 30 min, feature selection using KLD is 30 min, and segmentation using EM is 40 min, respectively, for 50 slices/patient on an INTEL Xeon CPU X5355 at 2.66 GHz and with 3.00 GB of RAM. Note that all these steps can be done off-line and made available to aid in a typical clinical setting wherein hundreds of MRI slices may be read by radiologists per day. In the future, we plan to extend our work for automated classification of tumor from nontumor regions after the PF tumor segmentation. Further, our

existing features may not be sufficient to discriminate among the brain tissues such asWM, GM, CSF from tumor, and edema. We need to investigate additional features for differentiating among tumor, nontumor, and edema. This will require fundamental work in extending KLD to discriminate multiclass tissues such as brain tissues, tumor, edema, and other artifacts in MRI.

ACKNOWLEDGMENT

The authors would like to thank Children's Hospital of Philadelphia for providing the pediatric brain MRI for this study.

REFERENCES

[1] A. W. C. Liew and H. Yan, "Current methods in the automatic tissue segmentation of 3D magnetic resonance brain images," *Current Med. Imag. Rev.*, vol. 2, no. 1, pp. 91–103, 2006.

[2] N. Sarkar and B. B. Chaudhuri, "An efficient approach to estimate fractal dimension of textural images," *Pattern Recog.*, vol. 25, pp. 1035–1041, 1992.

[3] P. M. Thompson, A. D. Lee, R. A. Dutton, J. A. Geaga, K. M. Hayashi, M. A. Eckert, U. Bellugi, A. M. Galaburda, J. R. Korenberg, D. L. Mills, A. W. Toga, and A. L. Reiss, "Abnormal cortical complexity and thickness profiles mapped in Williams syndrome," *J. Neurosci.*, vol. 25, no. 16, pp. 4146–4158, 2005.

[4] J. M. Zook and K. M. Iftekharuddin, "Statistical analysis of fractal-based brain tumor detection algorithms," *Magn. Resonance Imag.*, vol. 23, pp. 671–678, 2005.

[5] K. M. Iftekharuddin, A. Islam, J. Shaik, C. Parra, and R. Ogg, "Automatic brain tumor detection in MRI: Methodology and statistical validation," in *Proc. SPIE Symp. Med. Imag.*, 2005, vol. 5747, pp. 2012–2022.

[6] A. Islam, K. M. Iftekharuddin, R. Ogg, F. H. Laningham, and B. Sivakumar, "Multifractal modeling, segmentation, prediction and statistical validation of posterior fossa tumor," *SPIE Med. Imag. Conf.*, vol. 6915, pp. 69153C-1–69153C-12, Feb. 2008.

[7] K. M. Iftekharuddin, J. Zheng, M. A. Islam, and R. J. Ogg, "Fractal-based brain tumor detection in multimodal MRI," *Appl. Math. Comput.*, vol. 207, pp. 23–41, 2009.

[8] S. Osher and J. A. Sethian, "Fronts propagating with curvature dependent speed: Algorithms based on Hamilton–Jacobi formulation," *J. Comput. Phys.*, vol. 79, pp. 12–49, 1988.

[9] S. Suri, K. Liu, S. Singh, S. N. Laxminarayan, X. Zeng, and L. Reden, "Shape recovery algorithms using level sets in 2-D/3-D medical imagery: A state-of-the-art review," *IEEE Trans. Inf. Technol. Biomed.*, vol. 6, no. 1, pp. 8–28, Mar. 2002.

[10] G. Zhu, S. Zhang, Q. Zeng, and C. Wang, "Boundary-based image segmentation using binary level set method," *Opt. Eng.*, vol. 46, p. 050501, 2007.

[11] N. I. Weisenfield and S. K. Warfield, "Normalization of joint image-intensity statistics in MRI using the Kullback–Leibler divergence," in *Proc. IEEE Int. Symp. Biomed. Imag.: NanoMacro*, Apr. 15–18,, 2004, vol. 1, pp. 101–104.

[12] J. Novovicova, P. Pudil, and J. Kittler, "Divergence based feature selection for multimodal class densities," *IEEE trans. Pattern Anal. Mach. Intell.*, vol. 18, no. 2, pp. 218–223, Feb. 1996.

[13] A. Bru and J.M. Pastor, "Super-rough dynamics on tumor growth," *Phys. Rev. Lett.*, vol. 81, no. 18, pp. 4008–4011, 1998.

[14] J. Yu and Y. Wang, "Molecular image segmentation based on improved fuzzy clustering," *Int. J. Biomed. Imag.*, vol. 2007, p. 25182, 2007.

[15] V. Raad, "Design of Gabor wavelets for analysis of texture features in cervical imaging," in *Proc. IEEE 25th Annu. Int. Conf.*, Sep. 17–21, 2003, vol. 1, p. 806.

[16] Y. Zhan and D. Shen, "Deformable segmentation of 3D ultrasound prostrate images using statistical texture matching method," *IEEE Trans. Med. Imag.*, vol. 25, no. 3, pp. 256–272, Mar. 2006.

[17] C. Parra, K. M. Iftekharuddin, "Multiresolution-fractal feature extraction and tumor detection: Analytical modeling and implementation," presented at the 47th Annu. SPIE Meeting, Optical Science and Technology, San Diego, CA, 2003.

[18] S. Bidiwala and T. Pittman, "Neural network classification of pediatric posterior fossa tumors using clinical and imaging data," *J. Pediatric Neurosurgery*, vol. 40, pp. 8–15, 2004.

[19] X. Xu and A. Zhang, "Boost feature subset selection: A new gene selection algorithm for microarray dataset," *Int. J. Data Mining Bioinformatics*, vol. 3, 2009.

[20] I. Cohen, Q. Tan, X. S. Zhou, and T. S. Huang, "Feature selection using principal feature analysis," in *Proc. ACM Multimedia*, Augsburg, Germany, Sep. 23–29, 2007.

[21] E. Borenstein, E. Sharon, and S. Ullman, "Combining top down and bottom up segmentation," in *Proc. Conf. Comput. Vis. Patt. Recognit. Workshop (CVPRW)*, 2004, vol. 4, p. 48.

[22] M. Schaap, L. Neefjes, C. Metz, A. Giessen, A. Weustink, N. Mollet, J. Wentzel, T. Walsum, and W. Niessen, "Coronary lumen segmentation using graph cuts and robust kernel regression," *Inf. Process. Med. Imag.*, vol. 5636, pp. 528–539, 2009.

[23] S. Borman. (2004). "The expectation maximization algorithm-a short tutorial," [Online]. Available: http://www.seanborman.com/publications/EM_algorithm.pdf.

[24] B. B. Mandelbrot, *The Fractal Geometry of Nature*. San Francisco: Freeman, 1983.

[25] K. M. Iftekharuddin, W. Jia, and R. Marsh, "Fractal analysis of tumor in brain MR images," *Mach. Vis. Appl.*, vol. 13, pp. 352–362, 2003.

[26] G. W. Wornell and A. V. Oppenheim, "Wavelet based representation for a class of self similar signals with application to fractal modulation," *IEEE Trans. Inf. Theory*, vol. 38, no. 2, pp. 785–800, Mar. 1992.

[27] P. Goncalves, "Existence test of moments: Application to multifractal analysis," presented at the Int. Conf. of Telecommunications, Acapulco, Mexico, May 2000.

[28] K. M. Iftekharuddin, M. A. Islam, J. Shaik, C. Parra, and R. Ogg, "Automatic brain tumor detection in MRI: Methodology and statistical validation," *SPIE Med. Imag.*, vol. 5747, pp. 2012–2022, 2005.

Shaheen Ahmed received the B.S. degree from Vyavasayi Vidya Prathisthan Engineering College, Rajkot, Gujarat, India, and the M.S. degree from Wright State University, Dayton, OH. She is currently working toward the Ph.D. degree in electrical and computer engineering at the University of Memphis, Memphis, TN.

Her research interest includes image processing focusing on medical images, application of pattern recognition for analysis of MRI, and statistical methodologies.

Khan M. Iftekharuddin (SM'02) is an Associate Professor at the Department of Electrical and Computer Engineering, University of Memphis (UoM), Memphis, TN. He holds a joint appointment with the joint program in biomedical engineering at the UoM and University of Tennessee, Memphis. He also serves as a Faculty Member for the Bioinformatics Program and the Institute of Intelligent Systems, UoM. His research interests include medical image analysis, intelligent systems and reinforcement learning, computational modeling, bioinformatics, sensor signal and image analysis, computing and interconnection, automatic target recognition (ATR), and biologically inspired ATR. He is the principal author of more than 100 refereed journal papers,conference proceedings, and multiple book chapters. He obtained his B.Sc. degree from Bangladesh Institute of Technology in 1989. He received an M.S. and a Ph.D. both in electrical engineering from the University of Dayton in 1991 and 1995 respectively.

He serves as an Associate Editor for *Optical Engineering, International Journal of Image Processing and International Journal of Tomography and Statistics*. He is a Fellow of the SPIE, a Senior Member of the IEEE CIS in 2002, and a member of the OSA.

Arastoo Vossough's photograph and biography not available at the time of publication.